

# To what extents do urbanization and air pollution affect fog?

Shuqi Yan<sup>1,2,3,4</sup>, Bin Zhu<sup>1,2,3,4,\*</sup>, Yong Huang<sup>5,6</sup>, Jun Zhu<sup>7</sup>, Hanqing Kang<sup>1,2,3,4</sup>, Chunsong Lu<sup>1,2,3,4</sup>, Tong Zhu<sup>8</sup>

<sup>1</sup>Collaborative Innovation Center on Forecast and Evaluation of Meteorological Disasters, Nanjing University of Information Science & Technology, Nanjing, China

<sup>2</sup>Key Laboratory for Aerosol-Cloud-Precipitation of China Meteorological Administration, Nanjing University of Information Science & Technology, Nanjing, China

<sup>3</sup>Key Laboratory of Meteorological Disaster, Ministry of Education (KLME), Nanjing University of Information Science & Technology, Nanjing, China

<sup>4</sup>Special test field of National Integrated meteorological observation, Nanjing University of Information Science & Technology, Nanjing, China

<sup>5</sup>Anhui Meteorology Institute, Key Lab of Atmospheric Science and Remote Sensing Anhui Province, Hefei 230031, China

<sup>6</sup>Shouxian National Climatology Observatory, Shouxian 232200, China

<sup>7</sup>Xiangshan Meteorological Bureau, Xiangshan 315700, China

<sup>8</sup>IMSG at NOAA/NESDIS/STAR, 5830 University Research Ct., College Park, MD 20740, USA

*Correspondence to:* Bin Zhu (binzhu@nuist.edu.cn)

**Abstract.** The remarkable development of China has resulted in rapid urbanization (urban heat island and dry island) and severe air pollution (aerosol pollution). Previous studies demonstrate that these two factors have either suppressing or promoting effects on fog, but what are the extents of their individual and combined effects? In this study, a dense radiation fog event in East China in January 2017 was reproduced by the WRF-Chem model, and the individual and combined effects of urbanization and aerosols on fog (indicated by liquid water content (LWC)) are quantitatively revealed. Results show that urbanization inhibits low-level fog, delays its formation and advances its dissipation due to higher temperatures and lower saturations. In contrast, upper-level fog could be enhanced because of the updraft-induced vapour convergence. Aerosols promote fog by increasing LWC, increasing droplet concentration and decreasing droplet effective radius. Further experiments show that the current pollution level in China could be still below the critical aerosol concentration that suppresses fog. Urbanization influences fog to a larger extent than do aerosols. When urbanization and aerosol pollution are combined, the much weaker aerosol promoting effect is counteracted by the stronger urbanization suppressing effect on fog. Budget analysis of LWC reveals that urban development (urbanization and aerosols) alters LWC profile and fog structure mainly by modulating condensation/evaporation process. Our results infer that urban fog will be further reduced if urbanization keeps developing and air quality keeps deteriorating in the future.

# 31 1 Introduction

32 During the past five decades, China has achieved remarkable developments, accompanied by strong anthropogenic activities  
33 (rapid urbanization and severe air pollution). Urbanization and air pollution have significantly affected climate change,  
34 monsoons, air quality, fog, clouds and precipitation (e.g., Li et al., 2016; Li et al., 2017). Previous studies have linked the  
35 changes in clouds and precipitation to urbanization and aerosols. Urbanization destabilizes the boundary layer, which trig-  
36 gers strong updrafts and invigorates convection (e.g., Rozoff et al., 2003; Shepherd, 2005). Aerosols modify the macroscopic,  
37 microphysics, thermodynamics and radiative properties of clouds through complicated pathways, which are called as aero-  
38 sol-radiation and aerosol-cloud interactions and have been systematically reviewed by Fan et al. (2016), Rosenfeld et al.  
39 (2014), Tao et al. (2012), etc. Fog can be viewed as a cloud (Leng et al., 2014) that occurs near the surface. Land use features  
40 and aerosol properties may instantly affect fog, so fog is more sensitive to anthropogenic activities than other types of clouds  
41 are (Zhu and Guo, 2016). Previous studies have analysed the effects of urbanization and aerosols on fog, mostly in segregat-  
42 ed manners.

43 Urbanization is featured with urban heat island (UHI) and dry island (UDI) effects. The urban surface has a lower albedo,  
44 which reduces the reflected solar radiation and enhances heat storage. Urban expansion decreases the coverage of cropland,  
45 water bodies and forestland, which reduces the sources of water vapour. As a result, urban areas commonly experience high-  
46 er temperatures and lower vapour contents. These conditions induce a lower relative humidity that is unfavourable for fog  
47 formation (Gu et al., 2019). In the long-term scale, urban fog days are reported to decrease significantly (e.g., Guo et al.,  
48 2016; LaDochy, 2005; Sachweh and Koepke, 1995; Shi et al., 2008; Yan et al., 2019). Although UHI and UDI inhibit  
49 near-surface fog, the upward motions can promote upper-level fog (Li et al., 2011; Niu et al., 2010b). Surface roughness and  
50 thermal circulation cause strong updrafts (Rozoff et al., 2003), which transfer water vapour aloft and cause wet island phe-  
51 nomenon in the upper-level (Kang et al., 2014). The fog at that altitude may be subsequently enhanced.

52 Aerosols exert sophisticated impacts on fog through direct (radiation) effects and indirect (microphysical) effects (Khain and  
53 Pinsky, 2018). Aerosols attenuate shortwave radiation, influencing PBL structure and the vertical profile of moisture and  
54 aerosols (Tie et al., 2017, 2019), which can alter the formation and dissipation condition of fog. Scattering aerosols block  
55 downwelling solar radiation in the daytime, thus delaying the dissipation and elongating the duration of fog (Shi et al., 2008;  
56 Maalick et al., 2016). Although they increase downwelling longwave radiation at night, scattering aerosols have negligible  
57 effects on the fog formation time (Stolaki et al., 2015; Maalick et al., 2016). The role of absorbing aerosols like BC on fog  
58 depends on its residence height. If BC resides above the fog layer, BC causes a dome effect (Ding et al., 2016) which blocks  
59 solar radiation and prevents the dissipation of fog (Bott, 1991). If BC resides within the fog layer, BC heats fog droplets and  
60 accelerates the dissipation of fog (Maalick et al., 2016). The aerosol indirect effect on cloud is addressed as one of the most

61 uncertain factors in the IPCC report (IPCC, 2013). Aerosol concentration has a two-fold effect on fog, which is called as the  
62 boomerang pattern (Koren et al., 2008). Under saturation conditions, increasing aerosols commonly result in more CCNs. It  
63 promotes activation and condensation, yielding more but smaller droplets and increasing cloud water content (Fan et al.,  
64 2018; Rosenfeld et al., 2008). These changes have two kinds of positive feedback on fog (Maalick et al., 2016): more drop-  
65 lets cause stronger radiative cooling at fog top and enhance condensation (Jia et al., 2018); smaller droplet size inhibits sed-  
66 imentation and the depletion of cloud water (Zhang et al., 2014). However, if aerosol concentration exceeds a certain thresh-  
67 old, this promoting effect disappears (Quan et al., 2011) or even turns into a suppressing effect due to the strong vapour  
68 competition (Guo et al., 2017; Koren et al., 2008; Liu et al., 2019; Rangognio, 2009; Wang et al., 2015). Additionally,  
69 large-scale aerosol pollution can change weather patterns and affect large-scale fog formation conditions (Niu et al., 2010a).  
70 Ding et al. (2019) found that the dome effects of BC induce a land-sea thermal contrast and generate a cyclonic anomaly  
71 over coastal areas. This anomaly results in more vapor transported inland and strengthened advection-radiation fog.

72 Our recent observational work (Yan et al., 2019) indicated a decreasing trend in fog days, and the inhibiting effects of urban-  
73 ization outweigh the promoting effects of aerosols on fog during the mature urbanization stage. This study aims to quantita-  
74 tively confirm the roles of urbanization and aerosols in a dense fog event by an online-coupled synoptic and air quality mod-  
75 el, WRF-Chem. This event is a radiation fog event with weak synoptic forcing (detailed in Sect. 3.1), so the effects of urban-  
76 ization and aerosols should be obvious. Determining the quantitative extents of urbanization effect, aerosol effect and their  
77 combined effect is an interesting topic, which has barely been studied previously to the best of our knowledge. This work is  
78 expected to facilitate the understanding of how anthropogenic activities affect the natural environment, fog (cloud) physics  
79 and aerosol-cloud interactions near the surface.

80 In this study, urbanization mainly refers to UHI and UDI associated with land use change and human activities, excluding the  
81 increasing aerosol pollution caused by urban expansion. Air pollution refers to aerosols and is indicated by anthropogenic  
82 emissions because aerosol concentration is highly proportional to emission intensity. Liquid water content (LWC) and  
83 cloud/fog droplet number concentration ( $N_d$ ) are two important parameters representing fog intensity and visibility. Follow-  
84 ing previous studies (e.g., Ding et al., 2019; Gu et al., 2019; Jia et al., 2018; Maalick et al., 2016; Yang et al., 2018), we use  
85 LWC as the indicator of fog to reveal different characteristics of fog in different experiments. This study is organized as fol-  
86 lows. The data, model and methods are described in Sect. 2. Section 3.1 overviews the fog event and provides preliminary  
87 evidence of how urban development affects fog. Section 3.2 evaluates the model performance. Sections 3.3 to 3.5 analyse the  
88 urbanization, aerosol and combined effects on fog. Section 3.6 discusses the rationality and reliability of the results. Section  
89 4 concludes the findings of this study.

## 90 **2 Data, model and methods**

### 91 **2.1 Data**

92 The first data are the hourly automatic weather station data from the Shouxian National Climate Observatory (SX; 32.4° N,  
93 116.8° E, 23 m) that are used to evaluate the model performance. SX is a rural site surrounded by vast croplands and is ap-  
94 proximately 30 km away from the nearest large city, Huainan (Fig. 1b). The data include horizontal visibility, temperature,  
95 relative humidity, wind direction and speed. The second data are the Himawari 8 satellite data that are used to represent fog  
96 area (<https://www.eorc.jaxa.jp/tree/index.html>). Fog area is mainly indicated by the albedo at three visible bands: red (band  
97 3, 0.64  $\mu\text{m}$ ), green (band 2, 0.51  $\mu\text{m}$ ) and blue (band 1, 0.47  $\mu\text{m}$ ). The third data are the 3-hourly data from the Meteorologi-  
98 cal Information Comprehensive Analysis and Process System (MICAPS) (Li et al., 2010) that are also used to represent the  
99 fog area. The fourth data are the land use data from the Moderate Resolution Imaging Spectroradiometer Land Cover Type  
100 Version 6 data (MCD12Q1; <https://lpdaac.usgs.gov/products/mcd12q1v006>) in the year of 2017, the same as the simulation  
101 period. The data are resampled from 500 m to 30 arc-seconds (approximately 1 km) and used to replace the geological data  
102 of the WRF model.

### 103 **2.2 Model configuration**

104 The model used in this study is the WRF-Chem (V3.9.1.1) model. It is an online-coupled mesoscale synoptic and air quality  
105 model that considers the sophisticated interactions among various dynamic, physical and chemical processes (Chapman et al.,  
106 2009; Fast et al., 2006). WRF or WRF-Chem has been successfully used in simulating fog events (Jia and Guo, 2012; Jia and  
107 Guo, 2015; Jia et al., 2018) and exploring aerosol-cloud interactions (Fan et al., 2018). Two nest domains are set up (Fig. 1).  
108 The d01 domain has a size of 217 $\times$ 223 grids and a resolution of 6 km, covering the entire fog area of this event (Fig. 2a).  
109 The d02 domain has a size of 115 $\times$ 121 grids and a resolution of 2 km, covering SX and the adjacent areas. The land use data  
110 are replaced by MCD12Q1 data, which represent the latest condition.

111 Fog simulation is highly sensitive to vertical grids (Gultepe et al., 2007). A fine vertical resolution with a proper lowest  
112 model level can better resolve turbulences, thus yielding a reasonable fog structure (Yang et al., 2019). Here, 42 vertical lev-  
113 els are established with the first five  $\eta$  values of 1.000, 0.999, 0.998, 0.997, 0.996. There are 25 levels below the boundary  
114 layer (approximately 1500 m), and the lowest model level is approximately 8 m.

115 Fog simulation is also sensitive to physical schemes (Gu et al., 2019). Through numerous experiments, radiation, micro-  
116 physics and boundary schemes are found to significantly influence the model performance, and the boundary layer scheme  
117 plays a decisive role (Naira Chaouch et al., 2017). The radiation schemes are the RRTM longwave scheme and the Goddard

118 shortwave scheme. The microphysical scheme is the Morrison double-moment scheme (Morrison et al., 2005). The boundary  
119 layer scheme is the YSU 1.5-order closure non-local scheme, which yields better results than do any other schemes. The  
120 major schemes are listed in Tab. 1.

121 The model is driven by the highest resolution product (0.125°, approximately 13 km) of ECMWF data  
122 (<https://apps.ecmwf.int/datasets/data/interim-full-daily/levtype=sfc/>). The anthropogenic emissions are derived from the  
123 Multi-resolution Emission Inventory for China (MEIC) database (<http://www.meicmodel.org>). The simulation starts at  
124 2017-01-01 08:00 and ends at 2017-01-03 14:00, with the first 24 hours as the spin-up period (all the times here are in local  
125 time).

## 126 **2.3 Sensitivity experiments**

127 The study site is SX because only its visibility is observed hourly and is a multiple of 1 m, which is suitable for evaluating  
128 the model performance. To investigate the effects of urbanization and aerosols on fog, we change the land use and emission  
129 intensity around SX. Four experiments, i.e., u0e0, u3e0, u0e3 and u3e3 are designed. The u0e0 is the base experiment, with  
130 no urbanization and weak emission at SX. The u3e0 is set as the urbanization condition. The u0e3 is set as the polluted con-  
131 dition. The u3e3 is set as the urban development condition (urbanization and pollution coexist). The experiment settings are  
132 listed in Tab. 2.

133 On the setting of urbanized condition, we replace the land use of SX as that of Hefei, the most urbanized city and the capital  
134 of Anhui Province. The downtown of Hefei has a built area of approximately 570 km<sup>2</sup>. Therefore, the 11x13 box centered on  
135 SX (572 km<sup>2</sup>) is replaced by urban surface in the u3e0 and u3e3 experiments to represent the urbanization condition.

136 The downtown of Hefei has much higher emissions than SX. For example, the PM2.5 emission rate of Hefei is 40 times  
137 higher than that of SX. To represent the polluted condition, the emission intensity of the aforementioned box is set to be  
138 equal to that of downtown Hefei in the u0e3 and u3e3 experiments.

## 139 **2.4 Calculating visibility**

140 The LWC is the proxy of fog as mentioned above. Since the LWC is not observed, and visibility (VIS) is related to LWC, the  
141 VIS is used to assess the model performance. VIS is not diagnosed by the model and can be parameterized by the function of  
142 LWC, N<sub>d</sub> or droplet effective radius (R<sub>e</sub>). Equation 1 (Kunkel, 1983) and 2 (Gultepe et al, 2006) are two parameterization  
143 methods.

$$\text{VIS}[\text{m}] = 27 \text{LWC}[\text{g cm}^{-3}]^{-0.88} \quad (1)$$

$$\text{VIS}[\text{m}] = 1002(\text{LWC}[\text{g cm}^{-3}] \cdot \text{N}_d[\text{cm}^{-3}])^{-0.6473} \quad (2)$$

144 Another parameterization method is based on the Mie theory (Gultepe et al., 2017). VIS is inverse proportional to atmos-  
 145 pheric extinction at visible wavelength. The extinction coefficient of cloud water ( $\beta_c$ ) is

$$\beta_c [\text{km}^{-1}] = \frac{3Q_{\text{ext}} \rho_a \text{LWC}}{4\rho_w R_e} \times 10^6 \quad (3)$$

146 where  $\rho_a$  ( $\rho_w$ ) is the air (water) density in  $\text{kg m}^{-3}$ , LWC is in  $\text{g kg}^{-1}$ ,  $R_e$  is in  $\mu\text{m}$ , and  $Q_{\text{ext}}$  is the extinction efficiency, which is  
 147 assumed to be 2 for cloud droplets.

148 The atmospheric extinction ( $\beta$ ) is also largely contributed by aerosols ( $\beta_a$ ) and other types of hydrometeors. The model diag-  
 149 noses  $\beta_a$  at 550 nm. No other types of hydrometeors occur in this fog case, so we assume  $\beta = \beta_a + \beta_c$ . Then VIS is determined  
 150 by the Koschmieder rule (Koschmieder, 1924):  $\text{VIS}[\text{m}] = 3.912/\beta[\text{km}^{-1}] \times 1000$ .

151 During fog period (Fig. 4 shaded zone), the three methods nearly yield the same results (figure not shown), so the last meth-  
 152 od is used to calculate the simulated VIS.

## 153 **3 Results and discussions**

### 154 **3.1 Overview of the fog event**

#### 155 **3.1.1 Formation condition and lifetime**

156 From 01 to 06 January 2017, East China is dominated by zonal circulation, with weak trough, ridge, pressure gradient and  
 157 atmospheric diffusion (Zhang and Ma, 2017). Under this stable weather pattern, the accumulation of pollutants and water  
 158 vapour promote the occurrence of fog-haze events. From the evening of 02 January to the noon of 03 January, a dense fog  
 159 event occurs in wide regions of East China. The fog reaches its peak at 08:00 03 January, covering south Hebei, east Henan,  
 160 west Shandong, Anhui, Jiangsu and Shanghai (Fig. 2a). Figure 4a shows the temporal variation of visibility at SX. The fog  
 161 forms at 18:00 02 January and dissipates at 12:40 03 January. This is a radiation fog which is promoted by strong radiative  
 162 cooling at night and weak easterly water vapour transport from northwest Pacific (Zhu et al., 2019).

#### 163 **3.1.2 Preliminary evidence of urban development affecting fog**

164 Lee (1987) and Sachweh and Koepke (1995) observed "fog holes" over urban areas on satellite images. Here, fog hole means

165 the low liquid water path (LWP) region within the fog region, which is visualized as pixels with weak fog (high visibility) or  
166 clear sky surrounded by dense fog. These holes demonstrate that urban development (urbanization and aerosols) has a clear-  
167 ing effect on fog. In this fog event, fog holes are also present over urban areas on the Himawari 8 image at 11:00 03 January  
168 (Fig. 3). We assume that urbanization could have profound effects on fog by reducing the LWP or advancing the dissipation  
169 of fog, and the role of aerosols on fog is weaker than that of urbanization.

## 170 **3.2 Model evaluation and simulations**

171 The model performance is evaluated by comparing the fog spatial coverage. Satellite cloud image and modelled LWP ( $>2 \text{ g}$   
172  $\text{m}^{-2}$ ) can represent the observed and simulated fog zone, respectively (Jia et al., 2018). Figure 2 shows the Himawari 8 visible  
173 cloud image and the simulated LWP distribution at 08:00. The light white pixels and light red dots indicate the observed fog  
174 area. The model well captures the fog in south Hebei, east Henan, west Shandong, Anhui, Jiangsu and Shanghai.

175 The model performance is also evaluated by comparing the visibility and other basic parameters at the SX site (Fig. 4). Seen  
176 from the visibility, the simulated fog forms at 19:30, 1.5 h later than the observation, and dissipates at 12:20, 30 min earlier  
177 than the observation. During the fog period, the simulated visibility agrees well with the observation. The other parameters  
178 such as temperature, wind speed and relative humidity are also effectively reproduced by the model, with relative small  
179 RMSEs of 0.8 K, 0.7 m/s and 5.9 %, respectively. Overall, the model well captures the spatial feature and temporal evolution  
180 of the fog.

## 181 **3.3 Urbanization effects**

182 From different sensitivity experiments (u3e0, u0e3 and u3e3), we can deduce the extents of the separate or combined effects  
183 of urbanization and aerosols on fog. Figure 5 compares the LWC between u0e0 and u3e0. The general results are: (1) Before  
184 02:00, urbanization leads to a decreasing LWC in all layers. Fog forms on the surface at 22:30 in u3e0, 3 h later than in u0e0.  
185 (2) After 02:00, the LWC decreases in the low-level while it increases in the upper-level. Fog dissipates at 10:50 in u3e0, 1.5  
186 h earlier than in u0e0. To better explain the LWC difference, its profiles are shown in Fig. 6. At 23:00, although fog has  
187 formed in u3e0, the fog is rather weak compared with u0e0, which is caused by the higher temperature (Fig. 6f) and lower  
188 saturation associated with UHI and UDI. At 02:00, fog develops in u3e0, but its intensity (the value of LWC) cannot reach  
189 the same level as that in u0e0.

190 An interesting phenomenon is the opposite change of LWC in the low-level and upper-level after 02:00. This phenomenon  
191 can be explained by the role of updrafts. The increasing roughness length and extra warming in urban conditions could trig-  
192 ger horizontal wind convergence (Fig. S1) and the enhanced updrafts (Fig. 5c). The stronger updrafts in u3e0 affect conden-

193 sation via two possible pathways: (1) the vertical transport of vapour ( $-w \frac{\partial q}{\partial z}$ ) and vertical convergence/divergence ( $-q \frac{\partial w}{\partial z}$ ) re-  
194 distribute water vapour and affect condensation; (2) the adiabatic cooling promotes condensation. The role of the first path-  
195 way is measured by vertical vapour flux divergence ( $\frac{1}{g} \frac{\partial(qw)}{\partial z}$ ). At 05:00, u3e0 shows a stronger vapour convergence above 110  
196 m (Fig. 6h), and the LWC increases above 130 m (Fig. 6c). At 08:00, u3e0 shows a stronger vapour convergence above 130  
197 m (Fig. 6i), and the LWC increases above 170 m (Fig. 6d). Therefore, it is possible that the adiabatic cooling and up-  
198 draft-induced vapour flux convergence increase the vapour content and promote condensation in the upper-level, while the  
199 fog in the low-level is suppressed by the divergence of vapour flux. At 11:00, fog disappears at the ground in u3e0 likely due  
200 to the higher temperature (Fig. 6j). In summary, the UHI, UDI and updrafts alter the profile of LWC and reduce the LWP  
201 most of the time (Fig. 5c), and the decreasing LWP in the daytime can explain why fog holes occur above urban areas (Fig.  
202 3).

### 203 3.4 Aerosol effects

204 Figure 7 compares the LWC between u0e0 and u0e3. The formation time, dissipation time of fog and fog top show almost no  
205 changes. The LWC increases at almost all layers in the polluted condition. Accordingly, the LWP also increases (Fig. 7c). It  
206 is probable that the current pollution level of China always promotes fog occurrence. To testify whether the u0e3 is below  
207 the transition point of the boomerang pattern, eight additional experiments (D10, D7.5, D5, D2.5, M2.5, M5, M7.5 and M10)  
208 are performed. These experiments are the same as u0e3, except that the emissions around SX (the black box in Fig. 1b) are  
209 multiplied (the "M" prefix) or divided (the "D" prefix). For example, the name M2.5 means multiplying by 2.5; the name  
210 D10 means dividing by 10.

211 Figure 8 compares the LWC,  $N_d$ ,  $R_e$  and LWP among the nine emission-variant experiments. All the four parameters show  
212 the boomerang pattern, which demonstrates that the model is able to simulate the dual effects of aerosols. Below u0e3, the  
213 four parameters monotonically vary with emission level or CCN concentration, indicating that aerosol pollution could al-  
214 ways promote fog. This phenomenon is because stronger emissions produce more aerosols and CCN. Under saturation con-  
215 ditions, the larger amount of CCN boost activation and yield a higher  $N_d$ . The higher  $N_d$  reduces  $R_e$  and inhibits autoconver-  
216 sion and sedimentation (Twomey, 1977); thus, this situation decreases the depletion of fog water and increases the LWC.  
217 This promoting effect has been confirmed by previous model studies (e.g., Maalick et al., 2016; Stolaki et al., 2015) and ob-  
218 servations (e.g., Chen et al., 2012; Goren and Rosenfeld, 2012). The  $CCN_{0.1}$  concentration of u0e3 ( $570 \text{ cm}^{-3}$ ) is lower than  
219 that of the turning point (experiment M2.5) ( $1349 \text{ cm}^{-3}$ ), possibly indicating that the current pollution level in China (u0e3) is  
220 still located in the promoting regime rather than the suppressing regime of fog occurrence.

221 Rosenfeld et al. (2008) revealed that the turning point of boomerang pattern in convective clouds is  $CCN_{0.4} = 1200 \text{ cm}^{-3}$ . The



222 CCN<sub>0.4</sub> of u0e3 is 6023 cm<sup>-3</sup>, which seems to suppress fog. Aerosols affect convective clouds through two competing mech-  
 223 anisms: 1) invigorating convection by promoting vapour condensation. 2) suppressing convection by blocking solar radiation  
 224 and reducing surface heat flux. Under polluted conditions (AOD>0.3 or CCN<sub>0.4</sub>>1200 cm<sup>-3</sup>), the suppressing effect out-  
 225 weighs the invigoration effect, so the turning point occurs (Koren et al., 2008; Rosenfeld et al., 2008). This suppressing  
 226 effect does not exist in fog because fog commonly formed at night. Therefore, the turning point in fog might occur  
 227 later than that in convective clouds. In North China Plain where air pollution is thought to be more serious, a case  
 228 study by WRF-Chem also indicates that fog properties (e.g., LWC, N<sub>d</sub> and LWP) increase monotonically when emis-  
 229 sion intensity varies from 0.05-fold to 1-fold.

### 230 3.5 Combined effects of urbanization and aerosols

231 Figure 9 compares the LWC between u0e0 and u3e3. The u3e3-induced change is quite similar to but not the same as the  
 232 u3e0-induced change. The time-height average of absolute change of LWC induced by u3e0, u0e3 and u3e3 are 0.120, 0.019,  
 233 0.124 g kg<sup>-1</sup>, respectively. This result indicates that urbanization affects fog to a larger extent than do aerosols; when urbani-  
 234 zation and aerosols are combined, the effect of aerosols is indiscernible. The LWP is also significantly suppressed in the day-  
 235 time, and the promoting effect of aerosols in Fig. 7c is indiscernible in Fig. 9c. To further explain the changes in LWC, we  
 236 perform budget analysis of the LWC to determine which physical processes are the dominant contributors.

237 In WRF, the budget of LWC is composed of the following items,

$$238 \frac{\partial q_c}{\partial t} = - \underbrace{\left( u \frac{\partial}{\partial x} + v \frac{\partial}{\partial y} + w \frac{\partial}{\partial z} \right) q_c}_{\text{adv}} + \left( \frac{\partial q_c}{\partial t} \right)_{\text{PBL}} + \left( \frac{\partial q_c}{\partial t} \right)_{\text{micro}} + \left( \frac{\partial q_c}{\partial t} \right)_{\text{cumu}} \quad (4)$$

239 where  $q_c$  is LWC, and the subscripts denote advection, boundary layer, microphysical and cumulus processes, respectively.

240 The microphysical tendency is further decomposed into the following items,

$$241 \left( \frac{\partial q_c}{\partial t} \right)_{\text{micro}} = \left( \frac{\partial q_c}{\partial t} \right)_{\text{cold}} + \left( \frac{\partial q_c}{\partial t} \right)_{\text{auto}} + \left( \frac{\partial q_c}{\partial t} \right)_{\text{accr}} + \left( \frac{\partial q_c}{\partial t} \right)_{\text{sedi}} + \left( \frac{\partial q_c}{\partial t} \right)_{\text{cond/evap}} \quad (5)$$

242 where the subscripts denote cold phase processes, autoconversion, accretion, sedimentation and condensation/evaporation,  
 243 respectively.

244 All the processes regarding precipitation and cold phase (the cumu, cold, auto and accr subscripts) are not analysed because  
 245 no precipitation occurs, and the temperature is above 0°C in the simulated fog (figure not shown). The sum of microphysical

244 (condensation/evaporation and sedimentation), boundary layer and advection tendencies is equal to the LWC distribution, so  
245 the contributions of other physical processes can be safely ignored.

246 We can also infer that to what extents the various physical processes affect fog through the sensitivity experiments (u3e0,  
247 u0e3 and u3e3). Additional aerosols weakly influence these processes (Fig. S2 right column) and subsequently result in weak  
248 LWC change (Fig. 7c). Compared with aerosols, urbanization effect is much more considerable (Fig. S3 right column); it  
249 dominantly accounts for the variation in physical tendencies from u0e0 to u3e3 (Fig. 10 right column). In u3e3 condition,  
250 urban development (urbanization and aerosols) induces different magnitude of changes in different physical tendencies. The  
251 relative magnitudes are 52.1, 38.3 and 9.6 % for the microphysical, boundary layer and advection processes, respectively,  
252 indicating that microphysics is most susceptible to urban development and contributes most to the LWC change. Among  
253 various microphysical processes, condensation/evaporation contributes most (72.7 %) to the change in microphysical ten-  
254 dency (Fig. 11 right column). The above results indicate that urban development affects the LWC mainly by modulating the  
255 condensation/evaporation process. Since u3e3 condition still witnesses higher temperatures and stronger updrafts (figure not  
256 shown), the notable variation in condensation/evaporation tendency induced by u3e3 can also be attributed to the predomi-  
257 nant role of UHI, UDI and updrafts. The mechanism has been analysed in Sect. 3.3.

## 258 **3.6 Discussions**

259 As mentioned above, urbanization influences fog to a larger extent than do aerosols; the LWC in fog does not vary substan-  
260 tially with pollution level. This section discusses the rationality and reliability of our results through mechanism analysis and  
261 observational evidence.

262 The sensitivity of cloud properties to aerosols depends on aerosol concentration and saturation environment. In convective  
263 clouds with intense upward motions and high saturations, the response of cloud properties to additional aerosols is signifi-  
264 cant ("aerosol-limited regime") (Fan et al., 2018). However, in fog with much weaker updrafts and lower saturations, this  
265 response could be more sensitive to vapour content rather than aerosol concentration ("vapour-limited regime"). It possibly  
266 implies that the LWC in fog varies slightly with pollution level but considerably with saturation condition that related to ur-  
267 banization. Our results reveal that the time-height average LWC varies within the extent of  $0.07\text{g kg}^{-1}$  when emission inten-  
268 sity varies within two orders of magnitude (Fig. 8). This relative weak response of the LWC to pollution level is also report-  
269 ed by Jia et al. (2018).

270 In terms of observational evidence, Yan et al. (2019) revealed that fog days in polluted regions of East China have decreased  
271 since the 1990s. Through quantitative analysis, the promoting effects of aerosols are weakening, while the suppressing ef-  
272 fects of urbanization are enhancing and dominantly cause this decrease. Sachweh and Koepke (1995) also claimed that the

273 hindering effects of urbanization outweigh the promoting effects of aerosols on fog in southern Germany. Additionally, satel-  
274 lite images present discernible fog holes above urban areas (Fig. 3) (Lee, 1987; Sachweh and Koepke, 1995). Therefore,  
275 these observational evidence support the model results that the promoting effect of aerosols is counteracted by the hindering  
276 effect of urbanization. We believe that the results can also be applied to other large cities in China because these cities com-  
277 monly witness strong UHI, UDI and severe air pollution.

## 278 **4 Conclusions**

279 A dense radiation fog event occurred in East China from 02 to 03 January 2017. Satellite images show that fog holes occur  
280 over urban areas, demonstrating the remarkable effects of urbanization and air pollution on fog. Hence, the mechanism is  
281 investigated by the WRF-Chem model. The model well captures the spatial coverage and temporal evolution of the fog. Fur-  
282 thermore, the separate and combined effects of urbanization (refers to UHI and UDI) and air pollution (refers to aerosols) on  
283 fog (indicated by the LWC) are revealed, and the extents of these effects are quantitatively determined. Results show that:

284 Urbanization redistributes the LWC profile by the UHI, UDI effect and updrafts. The updrafts may be caused by surface  
285 roughness and extra warming. The UHI and UDI suppress low-level fog, delay its formation by 3 h, and advance its dissipa-  
286 tion by 1.5 h. However, the upper-level fog could be enhanced due to the updraft-induced adiabatic cooling and vapour flux  
287 convergence. Urbanization reduces the LWP most of the time, and this reduction in the daytime can explain why fog holes  
288 are present above urban areas on satellite images.

289 Aerosols promote fog mainly by changing microphysical properties. The increasing emissions (aerosol concentration) pro-  
290 duce more CCN and fog droplets, which decreases  $R_c$  and inhibits sedimentation, thus leading to a higher LWC. Further sen-  
291 sitivity experiments show that the current pollution level in China could be still below the transition point of the boomerang  
292 pattern that suppresses fog. The macroscopic properties such as fog top and lifetime remain nearly unchanged.

293 The role of urbanization far outweighs that of aerosols. Therefore, when they act together, the urbanization effect is domi-  
294 nant, and the aerosol effect is indiscernible. Budget analysis of LWC shows that increasing aerosols influence various physi-  
295 cal processes to a lesser extent, while urbanization influences these processes to a larger extent, eventually leading to a sub-  
296 stantial LWC change in urban development condition (urbanization and aerosols). In this condition, the comparisons among  
297 various physical processes reveal that microphysics dominates the change in LWC, and condensation/evaporation dominates  
298 the change in microphysical tendency. This result highlights the importance of condensation/evaporation process in modu-  
299 lating the LWC profile and fog structure.

300 Mechanism analysis and the observational evidence support our key finding that urbanization influences fog to a much larger

301 extent than do aerosol pollution. Therefore, we believe our results are reasonable and robust in radiation fog events without  
302 strong synoptic forcings, and the results can also be applied to other large cities in China due to the similar urban develop-  
303 ment patterns. This study is expected to facilitate a better understanding of how anthropogenic activities affect the natural  
304 environment, fog (cloud) physics and aerosol-cloud interactions near the surface. We can also infer the future change of fog  
305 occurrence. Under the traditional urban development pattern, i.e., urbanization keeps developing and air quality keeps dete-  
306 riorating, urban fog occurrence will be further reduced.

307

308 *Code and data availability.* Some of the data repositories have been listed in Sect. 2. The other data, model outputs and  
309 codes can be accessed by contacting Bin Zhu via [binzhu@nuist.edu.cn](mailto:binzhu@nuist.edu.cn).

310

311 *Author contributions.* SY performed the model simulation, data analysis and manuscript writing. BZ proposed the idea, su-  
312 pervised this work and revised the manuscript. YH provided the observation data at the SX site. JZ processed the observation  
313 data. HK offered helps to the model simulation. CL and TZ also contributed to the manuscript revision.

314

315 *Competing interests.* The authors declare that they have no conflict of interest.

316

317 *Acknowledgments.* We are grateful to the High Performance Computing Center of Nanjing University of Information Science  
318 and Technology for doing the numerical calculations in this work on its blade cluster system. We thank American Journal  
319 Experts (AJE) for the English language editing.

320

321 *Financial support.* This work is supported by the National Key Research and Development Program (2016YFA0602003)  
322 and the National Natural Science Foundation of China (91544229, 41575148, 41605091).

## 323 **References**

- 324 Abdul-Razzak, H. and Ghan, S. J.: A parameterization of aerosol activation 3. Sectional representation, *J. Geophys. Res.*, 107,  
325 AAC-1-AAC 1-6, <https://doi.org/10.1029/2001jd000483>, 2002.
- 326 Bott, A.: On the influence of the physico-chemical properties of aerosols on the life cycle of radiation fogs, *J. Aerosol. Sci.*, 21, 1–31,  
327 <https://doi.org/10.1007/BF00119960>, 1991.

328 Chapman, E. G., Gustafson, W. I., Easter, R. C., Barnard, J. C., Ghan, S. J., and Pekour, M. S.: Coupling aerosol-cloud-radiative processes  
329 in the WRF-Chem model: Investigating the radiative impact of elevated point sources, *Atmos. Chem. Phys.*, 9, 945–964,  
330 <https://doi.org/10.5194/acp-9-945-2009>, 2009.

331 Chen, Y. C., Christensen, M. W., Xue, L., Sorooshian, A., Stephens, G. L., Rasmussen, R. M., and Seinfeld, J. H.: Occurrence of lower  
332 cloud albedo in ship tracks, *Atmos. Chem. Phys.*, 12, 8223–8235, <https://doi.org/10.5194/acp-12-8223-2012>, 2012.

333 Di Vittorio, A. V. and Emery, W. J.: An automated, dynamic threshold cloud-masking algorithm for daytime AVHRR images over land,  
334 *IEEE Trans. Geosci. Remote Sensing*, 40, 1682–1694, <https://doi.org/10.1109/TGRS.2002.802455>, 2002.

335 Ding, A. J., Huang, X., Nie, W., Sun, J. N., Kerminen, V. - M., Petäjä, T., Su, H., Cheng, Y. F., Yang, X. - Q., Wang, M. H., Chi, X. G.,  
336 Wang, J. P., Virkkula, A., Guo, W. D., Yuan, J., Wang, S. Y., Zhang, R. J., Wu, Y. F., Song, Y., Zhu, T., Zilitinkevich, S., Kulmala, M.,  
337 and Fu, C. B.: Enhanced haze pollution by black carbon in megacities in China, *Geophys. Res. Lett.*, 43, 2873–2879,  
338 <https://doi.org/10.1002/2016gl067745>, 2016.

339 Ding, Q., Sun, J., Huang, X., Ding, A., Zou, J., Yang, X., and Fu, C.: Impacts of black carbon on the formation of advection–radiation fog  
340 during a haze pollution episode in eastern China, *Atmos. Chem. Phys.*, 19, 7759–7774, <https://doi.org/10.5194/acp-19-7759-2019>,  
341 2019.

342 Fan, J., Rosenfeld, D., Zhang, Y., Giangrande, S. E., Li, Z., and Machado, L. A. T.: Substantial convection and precipitation enhancements  
343 by ultrafine aerosol particles, *Science*, 359, 411–418, <https://doi.org/10.1126/science.aan8461>, 2018.

344 Fan, J., Wang, Y., Rosenfeld, D., and Liu, X.: Review of Aerosol–Cloud Interactions: Mechanisms, Significance, and Challenges, *J. Atmos.*  
345 *Sci.*, 73, 4221–4252, <https://doi.org/10.1175/JAS-D-16-0037.1>, 2016.

346 Fast, J. D., Gustafson, W. I., Easter, R. C., Zaveri, R. A., Barnard, J. C., Chapman, E. G., Grell, G. A., and Peckham, S. E.: Evolution of  
347 ozone, particulates, and aerosol direct radiative forcing in the vicinity of Houston using a fully coupled meteorolo-  
348 gy-chemistry-aerosol model, *J. Geophys. Res.*, 111, <https://doi.org/10.1029/2005jd006721>, 2006.

349 Goren, T. and Rosenfeld, D.: Satellite observations of ship emission induced transitions from broken to closed cell marine stratocumulus  
350 over large areas, *J. Geophys. Res.-Atmos.*, 117, -, <https://doi.org/10.1029/2012JD017981>, 2012.

351 Gu, Y., Kusaka, H., van Doan, Q., and Tan, J.: Impacts of urban expansion on fog types in Shanghai, China: Numerical experiments by  
352 WRF model, *Atmos. Res.*, 220, 57–74, <https://doi.org/10.1016/j.atmosres.2018.12.026>, 2019.

353 Gultepe, I., Tardif, R., Michaelides, S. C., Cermak, J., Bott, A., Bendix, J., Müller, M. D., Pagowski, M., Hansen, B., Ellrod, G., Jacobs, W.,  
354 Toth, G., and Cober, S. G.: Fog Research: A Review of Past Achievements and Future Perspectives, *Pure Appl. Geophys.*, 164, 1121–  
355 1159, <https://doi.org/10.1007/s00024-007-0211-x>, 2007.

356 Gultepe, I., Müller, M. D., and Boybeyi, Z.: A New Visibility Parameterization for Warm-Fog Applications in Numerical Weather Predic-  
357 tion Models, *J. Appl. Meteorol. Climatol.*, 45, 1469–1480, <https://doi.org/10.1175/jam2423.1>, 2006.

358 Gultepe, I., Milbrandt, J. A., and Zhou, B.: Marine fog: A review on microphysics and visibility prediction, in: Koračin D., Dorman C. (eds)  
359 *Marine Fog: Challenges and Advancements in Observations, Modeling, and Forecasting*, Springer, Cham, 50 pp., 2017.

360 Guo, J., Su, T., Li, Z., Miao, Y., Li, J., Liu, H., Xu, H., Cribb, M., and Zhai, P.: Declining frequency of summertime local-scale precipita-  
361 tion over eastern China from 1970 to 2010 and its potential link to aerosols, *Geophys. Res. Lett.*, 44, 5700–5708,  
362 <https://doi.org/10.1002/2017GL073533>, 2017.

363 Guo, T., Zhu, B., Kang, Z., Gui, H., and Kang, H.: Spatial and temporal distribution characteristic of fog days and haze days from  
364 1960~2012 and impact factors over the Yangtze River Delta Region, China *Environmental Science*, 36, 961 – 969,  
365 <https://doi.org/10.3969/j.issn.1000-6923.2016.04.001>, 2016. [in Chinese]

366 IPCC: Climate change 2013: The physical science basis, Contribution of Working Group I to the Fifth Assessment Report of the Intergov-  
367 ernmental Panel on Climate Change, Cambridge University Press, Cambridge, United Kingdom and New York, NY, USA, 1585 pp.,  
368 2013.

369 Jia, X. and Guo X.: Impacts of Anthropogenic Atmospheric Pollutant on Formation and Development of a Winter Heavy Fog Event, Chi-  
370 nese Journal of Atmospheric Sciences, 36, 995– 1008, <https://doi.org/10.3878/j.issn.1006-9895.2012.11200>, 2012. [in Chinese]

371 Jia, X. and Guo, X.: Impacts of Secondary Aerosols on a Persistent Fog Event in Northern China, *Atmospheric and Oceanic Science Letters*, 5, 401–407, <https://doi.org/10.1080/16742834.2012.11447022>, 2015.

372

373 Jia, X., Quan, J., Zheng, Z., Liu, X., Liu, Q., He, H., and Liu, Y.: Impacts of anthropogenic aerosols on fog in North China Plain, *J. Geophys. Res.-Atmos.*, 124, 252–265, <https://doi.org/10.1029/2018jd029437>, 2018.

374

375 Kang, H., Zhu, B., Zhu, T., Sun, J., and Ou, J.: Impact of Megacity Shanghai on the Urban Heat-Island Effects over the Downstream City Kunshan, *Bound.-Layer Meteor.*, 152, 411–426, <https://doi.org/10.1007/s10546-014-9927-1>, 2014.

376

377 Khain, A. P. and Pinsky, M.: Modeling: A Powerful Tool for Cloud Investigation, in: *Physical processes in clouds and cloud modeling*, Cambridge University Press, Cambridge, United Kingdom and New York, NY, USA, 98 pp., 2018.

378

379 Koren, I., Martins, J. V., Remer, L. A., and Afargan, H.: Smoke invigoration versus inhibition of clouds over the Amazon, *Science*, 321, 946–949, <https://doi.org/10.1126/science.1159185>, 2008.

380

381 Koschmieder, H.: Theorie der horizontalen sichtweite, *Beitr Phys.d.freien Atm*, 12, 171–181, 1924.

382

383 Kunkel, B. A.: Parameterization of Droplet Terminal Velocity and Extinction Coefficient in Fog Models, *J. Appl. Meteorol.*, 23, 34–41, [https://doi.org/10.1175/1520-0450\(1984\)023<0034:PODTVA>2.0.CO;2](https://doi.org/10.1175/1520-0450(1984)023<0034:PODTVA>2.0.CO;2), 1983

384

385 LaDochy, S.: The Disappearance of Dense Fog in Los Angeles: Another Urban Impact?, *Phys. Geogr.*, 26, 177–191, <https://doi.org/10.2747/0272-3646.26.3.177>, 2005.

386

387 Lee, T. F.: Urban clear islands in California central valley fog, *Mon. Weather Rev.*, 115, 1794–1796, [https://doi.org/10.1175/1520-0493\(1987\)1152.0.CO;2](https://doi.org/10.1175/1520-0493(1987)1152.0.CO;2), 1987.

388

389 Leng, C., Zhang, Q., Zhang, D., Xu, C., Cheng, T., Zhang, R., Tao, J., Chen, J., Zha, S., and Zhang, Y.: Variations of cloud condensation nuclei (CCN) and aerosol activity during fog-haze episode: a case study from Shanghai, *Atmos. Chem. Phys.*, 14, 12499–12512, <https://doi.org/10.5194/acp-14-12499-2014>, 2014.

390

391 Li, Y., Cao, L., Gao, S., and Luo, B.: The Current Stage and Development of MICAPS, *Meteorological Monthly*, 36, 50-55, 2010. [in Chinese]

392

393 Li, Z., Guo, J., Ding, A., Liao, H., Liu, J., Sun, Y., Wang, T., Xue, H., Zhang, H., and Zhu, B.: Aerosol and boundary-layer interactions and impact on air quality, *Natl. Sci. Rev.*, 4, 810–833, <https://doi.org/10.1093/nsr/nwx117>, 2017.

394

395 Li, Z., Lau, W. K. M., Ramanathan, V., Wu, G., Ding, Y., Manoj, M. G., Liu, J., Qian, Y., Li, J., Zhou, T., Fan, J., Rosenfeld, D., Ming, Y., Wang, Y., Huang, J., Wang, B., Xu, X., Lee, S. S., Cribb, M., Zhang, F., Yang, X., Zhao, C., Takemura, T., Wang, K., Xia, X., Yin, Y., Zhang, H., Guo, J., Zhai, P. M., Sugimoto, N., Babu, S. S., and Brasseur, G. P.: Aerosol and monsoon climate interactions over Asia, *Rev. Geophys.*, 54, 866–929, <https://doi.org/10.1002/2015RG000500>, 2016.

396

397

398

399 Li, Z., Yang, J., Shi, C., and Pu, M.: Urbanization Effects on Fog in China: Field Research and Modeling, *Pure Appl. Geophys.*, 169, 927–939, <https://doi.org/10.1007/s00024-011-0356-5>, 2011.

400

401 Liu, H., Guo, J., Koren, I., Altaratz, O., Dagan, G., Wang, Y., Jiang, J. H., Zhai, P., and Yung, Y. L.: Non-Monotonic Aerosol Effect on precipitation in Convective Clouds over tropical oceans. *Sci. Rep.*, 9, 1-7, <https://doi.org/10.1038/s41598-019-44284-2>, 2019.

402

403 Maalick, Z., Kühn, T., Korhonen, H., Kokkola, H., Laaksonen, A., and Romakkaniemi, S.: Effect of aerosol concentration and absorbing aerosol on the radiation fog life cycle, *Atmos. Environ.*, 133, 26–33, <https://doi.org/10.1016/j.atmosenv.2016.03.018>, 2016.

404

405 Morrison, H., Curry, J. A., and Khvorostyanov, V. I.: A new double-moment microphysics parameterization for application in cloud and climate models. Part I: Description, *J. Atmos. Sci.*, 62, 1665–1677, <https://doi.org/10.1175/JAS3446.1>, 2005.

406

407 Naira Chaouch, Marouane Temimi, Michael Weston, and Hosni Ghedira: Sensitivity of the meteorological model WRF-ARW to planetary boundary layer schemes during fog conditions in a coastal arid region, *Atmos. Res.*, 187, 106–127, <https://doi.org/10.1016/j.atmosres.2016.12.009>, available at: <http://www.sciencedirect.com/science/article/pii/S0169809516307116>, 2017.

408

409

410

411 Niu, F., Li, Z., Li, C., Lee, K., and Wang, M.: Increase of wintertime fog in China: Potential impacts of weakening of the Eastern Asian monsoon circulation and increasing aerosol loading, *J. Geophys. Res.*, 115, <https://doi.org/10.1029/2009jd013484>, 2010a.

412

413 Niu, S., Lu, C., Yu, H., Zhao, L., and Lü, J.: Fog research in China: An overview, *Adv. Atmos. Sci.*, 27, 639–662, <https://doi.org/10.1007/s00376-009-8174-8>, 2010b.

414

415 Rangognio, J.: Influence of aerosols on the formation and development of radiation fog, *Atmos. Chem. Phys.*, 9, 17963–18019,  
416 <https://doi.org/10.5194/acpd-9-17963-2009>, 2009.

417 Rosenfeld, D., Meinrat O. Andreae, Asmi, A., Chin, M., and Johannes Quaas: Global observations of aerosol-cloud-precipitation-climate  
418 interactions, *Rev. Geophys.*, 52, 750–808, <https://doi.org/10.1002/2013RG000441>, 2014.

419 Rosenfeld, D., Lohmann, U., Raga, G. B., O’Dowd, C. D., Kulmala, M., Fuzzi, S., Reissell, A., and Andreae, M. O.: Flood or drought:  
420 how do aerosols affect precipitation?, *Science*, 321, 1309–1313, <https://doi.org/10.1126/science.1160606>, 2008.

421 Rozoff, C. M., Cotton, W. R., and Adegoke, J. O.: Simulation of St. Louis, Missouri, Land Use Impacts on Thunderstorms, *J. Appl. Mete-*  
422 *orol.*, 42, 716–738, [https://doi.org/10.1175/1520-0450\(2003\)042<0716:SOSLML>2.0.CO;2](https://doi.org/10.1175/1520-0450(2003)042<0716:SOSLML>2.0.CO;2), 2003.

423 Sachweh, M. and Koepke, P.: Radiation fog and urban climate, *Geophys. Res. Lett.*, 22, 1073–1076, <https://doi.org/10.1029/95gl00907>,  
424 1995.

425 Shepherd, J. M.: A Review of Current Investigations of Urban-Induced Rainfall and Recommendations for the Future, *Earth Interact.*, 9,  
426 1–27, <https://doi.org/10.1175/ei156.1>, 2005.

427 Shi, C., Roth, M., Zhang, H., and Li, Z.: Impacts of urbanization on long-term fog variation in Anhui Province, China, *Atmos. Environ.*, 42,  
428 8484–8492, <https://doi.org/10.1016/j.atmosenv.2008.08.002>, 2008.

429 Stolaki, S., Haeffelin, M., Lac, C., Dupont, J. C., Elias, T., and Masson, V.: Influence of aerosols on the life cycle of a radiation fog event.  
430 A numerical and observational study, *Atmos. Res.*, 151, 146–161, <https://doi.org/10.1016/j.atmosres.2014.04.013>, 2015.

431 Tao, W. K., Chen, J. P., Li, Z., Wang, C., and Zhang, C.: Impact of aerosols on convective clouds and precipitation, *Rev. Geophys.*, 50,  
432 6837, <https://doi.org/10.1029/2011RG000369>, 2012.

433 Tie, X., Huang, R., Cao, J., Zhang, Q., Cheng, Y., Su, H., Chang, D., Pöschl, U., Hoffmann, T., Dusek, U., Li, G., Worsnop, D., and  
434 O’Dowd, C.: Severe Pollution in China Amplified by Atmospheric Moisture, *Sci. Rep.* 7, 15760,  
435 <https://doi.org/10.1038/s41598-017-15909-1>, 2017.

436 Tie, X., Long, X., Li, G., Zhao, S., Cao, J., and Xu, J.: Ozone enhancement due to photo-dissociation of nitrous acid in eastern China, *At-*  
437 *mos. Chem. Phys.*, 19, 11267–11278, <https://doi.org/10.5194/acp-19-11267-2019>, 2019.

438 Twomey, S. A.: The Influence of Pollution on the Shortwave Albedo of Clouds, *J. Atmos. Sci.*, 34, 1149–1154,  
439 [https://doi.org/10.1175/1520-0469\(1977\)034<1149:tiopot>2.0.co;2](https://doi.org/10.1175/1520-0469(1977)034<1149:tiopot>2.0.co;2), 1977.

440 Wang, F., Guo, J., Zhang, J., Huang, J., Min, M., Chen, T., Liu, H., Deng, M., and Li, X.: Multi-sensor quantification of aerosol-induced  
441 variability in warm clouds over eastern China, *Atmos. Environ.*, 113, 1–9, <https://doi.org/10.1016/j.atmosenv.2015.04.063>, 2015

442 Yan, S., Zhu, B., and Kang, H.: Long-term fog variation and its impact factors over polluted regions of East China, *J. Geophys.*  
443 *Res.-Atmos.*, 124, 1741–1754, <https://doi.org/10.1029/2018JD029389>, 2019.

444 Yang, Y., Hu, X., Gao, S., and Wang, Y.: Sensitivity of WRF simulations with the YSU PBL scheme to the lowest model level height for a  
445 sea fog event over the Yellow Sea, *Atmos. Res.*, 215, 253–267, <https://doi.org/10.1016/j.atmosres.2018.09.004>, 2019.

446 Zhang, N. and Ma, X.: Analysis of the June 2018 Atmospheric Circulation and Weather, *Meteorological Monthly*, 43, 508– 512,  
447 <https://doi.org/10.7519/j.issn.1000-0526.2017.04.014>, 2017. [in Chinese]

448 Zhang, X., Musson-Genon, L., Dupont, E., Milliez, M., and Carissimo, B.: On the Influence of a Simple Microphysics Parametrization on  
449 Radiation Fog Modelling: A Case Study During ParisFog, *Bound.-Layer Meteor.*, 151, 293–315,  
450 <https://doi.org/10.1007/s10546-013-9894-y>, 2014.

451 Zhu, B. and Guo, T.: Review of the Impact of Air Pollution on Fog, *Advances in Meteorological Science and Technology*, 6, 56– 63,  
452 <https://doi.org/10.3969/j.issn.2095-1973.2016.02.006>, 2016. [in Chinese]

453 Zhu, J., Zhu, B., Huang, Y., An, J., and Xu, J.: PM2.5 vertical variation during a fog episode in a rural area of the Yangtze River Delta,  
454 China, *Sci. Total. Environ.*, 685, 555–563, <https://doi.org/10.1016/j.scitotenv.2019.05.319>, 2019.

455

456 Table 1. Summary of major parameterization schemes.

Scheme	Option
Boundary layer	YSU
Longwave radiation	RRTM
Shortwave radiation	New Goddard
Microphysics	Morrison
Surface layer	MM5 similarity
Land surface	Noah
Urban surface	Urban canopy model
Gas phase chemistry	CBMZ
Aerosol chemistry	MOSAIC (4-bin)
Aerosol-cloud and aerosol-radiation interactions	All turned on
Aerosol activation	Abdul-Razzak and Ghan (2002)

457

458



459 Table 2. Settings of sensitive experiments. "N" represents no changes.

Case name	Description	Underlying surface	Anthropogenic emission
u0e0	base condition	N	N
u3e0	urbanization condition	the 11x13 grid centered on SX is replaced by urban surface	N
u0e3	polluted condition	N	the 11x13 grid centered on SX is replaced by the emission of Hefei downtown
u3e3	urbanization and polluted condition	same as u3e0	same as u0e3

Effect	Description
u3e0-u0e0	urbanization effect
u0e3-u0e0	aerosol effect
u3e3-u0e0	urbanization and aerosol effect

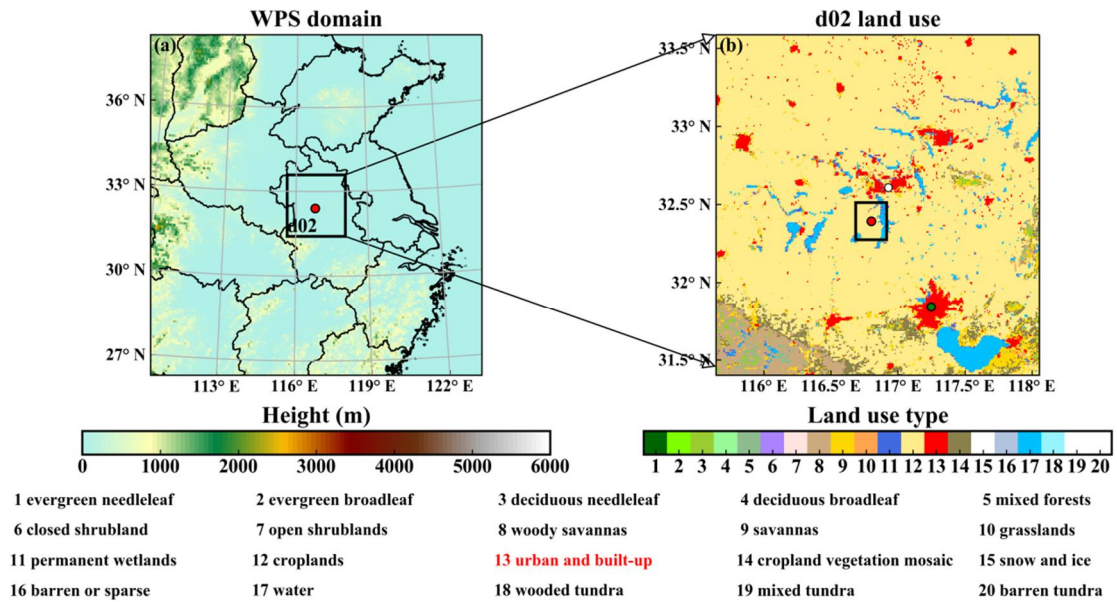
460

461

462

463

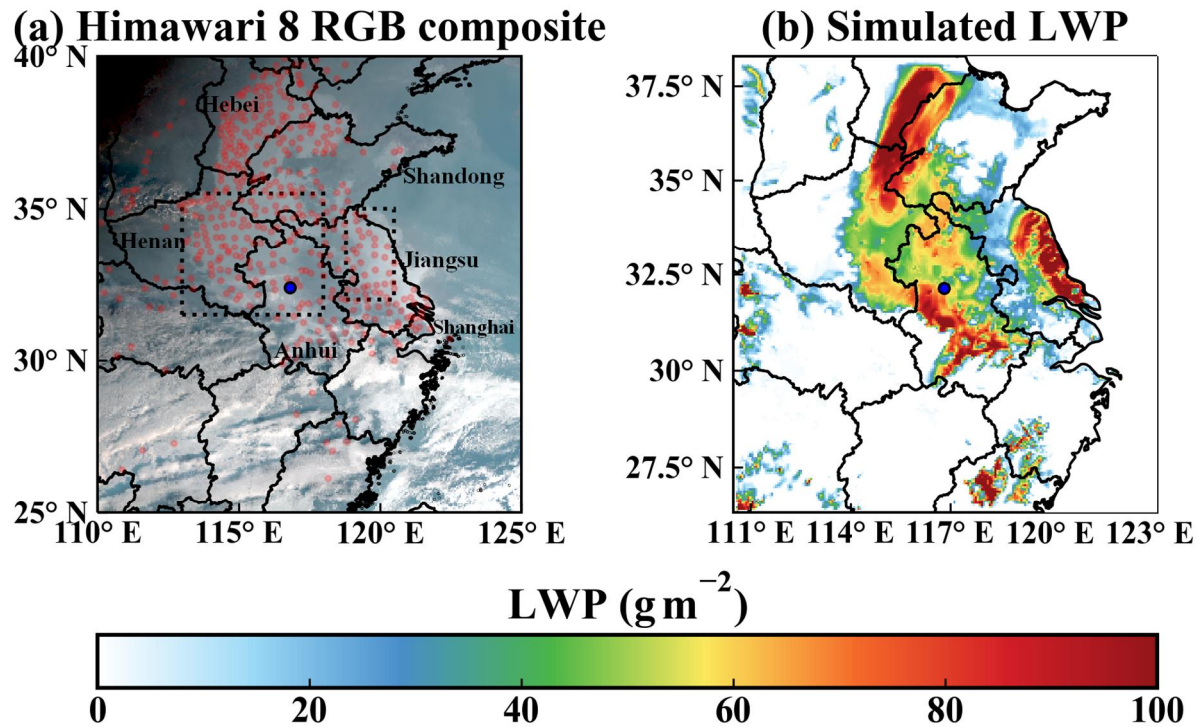
464



466

467 Figure 1. (a) The WRF domain overlaid with terrain height. (b) The land use distribution of domain d02. The green dot is Hefei, the capital of Anhui Province. The white dot is Huainan. The two red dots are the SX site. The land use and  
 468 emissions of the 22 km × 26 km black box in the center of (b) will be altered in the sensitivity experiments.

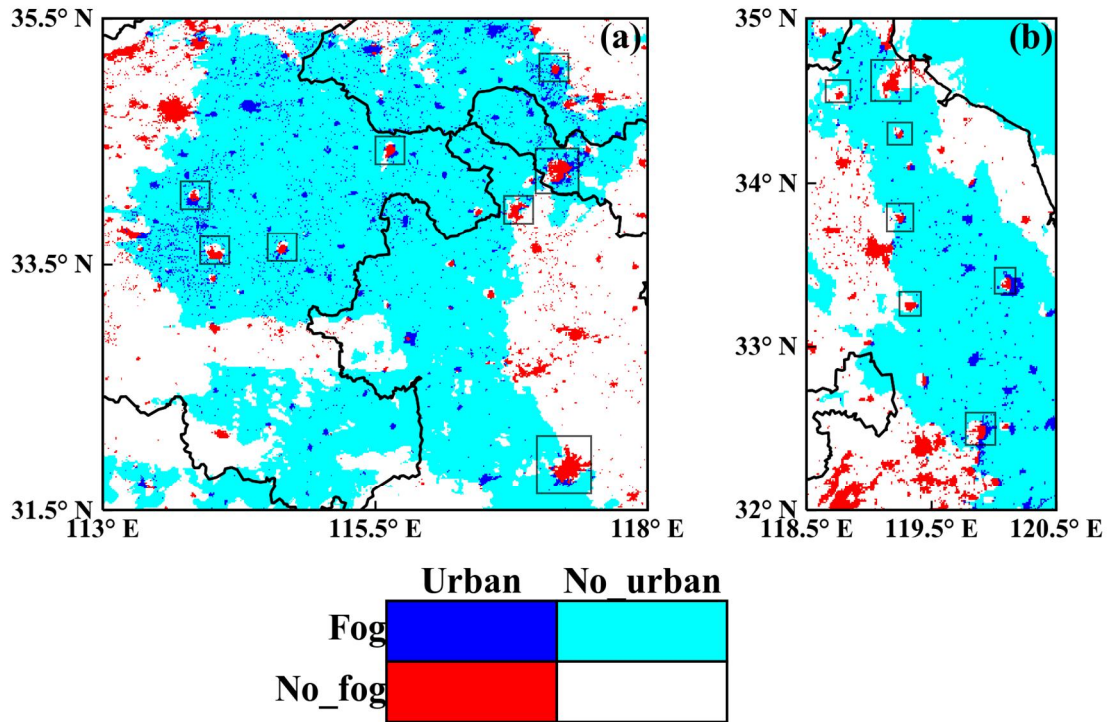
470



472

473 Figure 2. The performance of the simulated fog zone at 08:00 03 January 2017. (a) Himawari 8 RGB composite cloud  
 474 image overlaid with the MICAPS observation sites (light red dots) at which fog was observed (relative humidity > 90 %  
 475 and VIS < 1 km). (b) Simulated LWP distribution. Only LWC below 1500 m are integrated. The blue dots are the SX  
 476 site. The two dashed rectangles in (a) are the subregions of interest in Fig. 3.

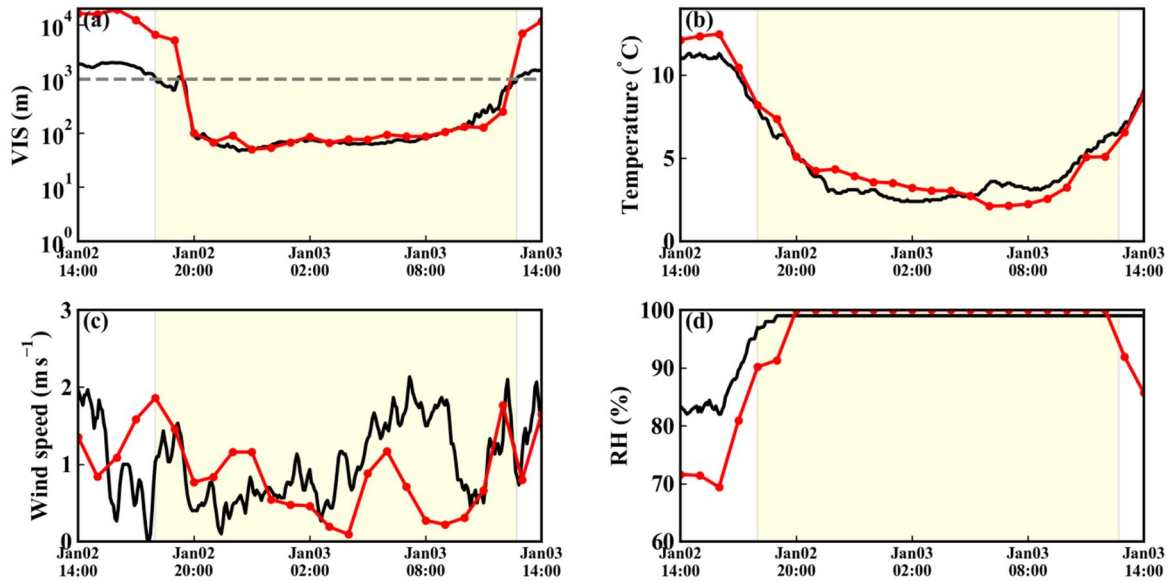
477



479

480 Figure 3. Two sub-regions (a and b) with obvious fog holes on the Himawari 8 image at 11:00 03 January 2017. The  
 481 fog zone, which is represented by albedo > 0.45 (at 0.64  $\mu\text{m}$ ) and brightness temperature > 266 K (at 12.4  $\mu\text{m}$ ) (Di  
 482 Vittorio et al., 2002), is marked with cold colours (blue or cyan). The urban areas are marked with blue or red. The red  
 483 and white pixels surrounded or semi-surrounded by cold colours are fog holes, and among these pixels, the red pixels  
 484 indicate the fog holes over urban areas. Some of the cities with fog holes are marked by rectangles.

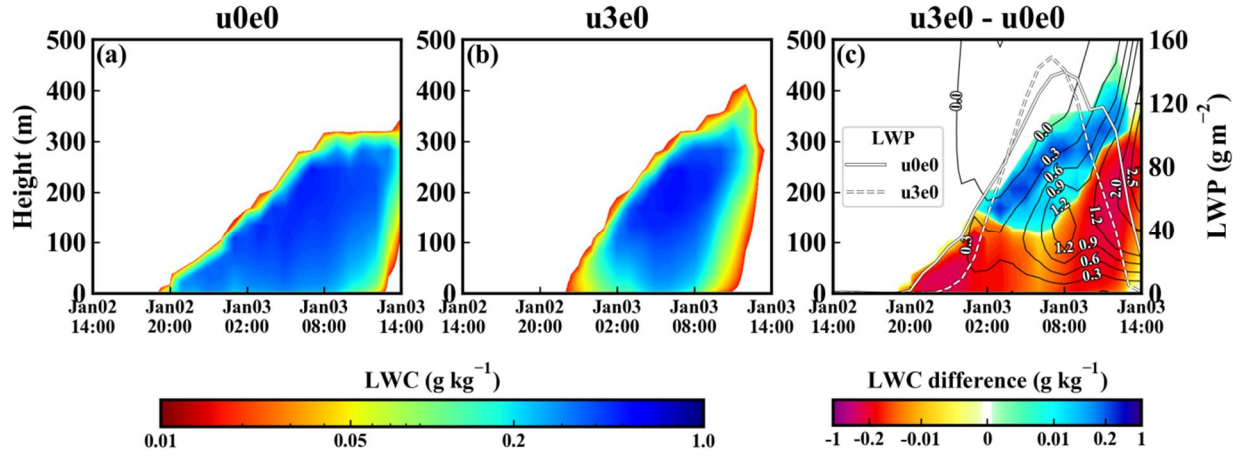
485



487

488 Figure 4. The performance of the simulated meteorological parameters at the SX site. (a) VIS. (b) air temperature. (c)  
 489 10-minute average wind speed. (d) Relative humidity (RH). The red dotted lines represent the model results, and the  
 490 black lines are the observations. The fog period ( $\text{VIS} < 1 \text{ km}$  and  $\text{RH} > 90 \%$ ) is shaded with light yellow.

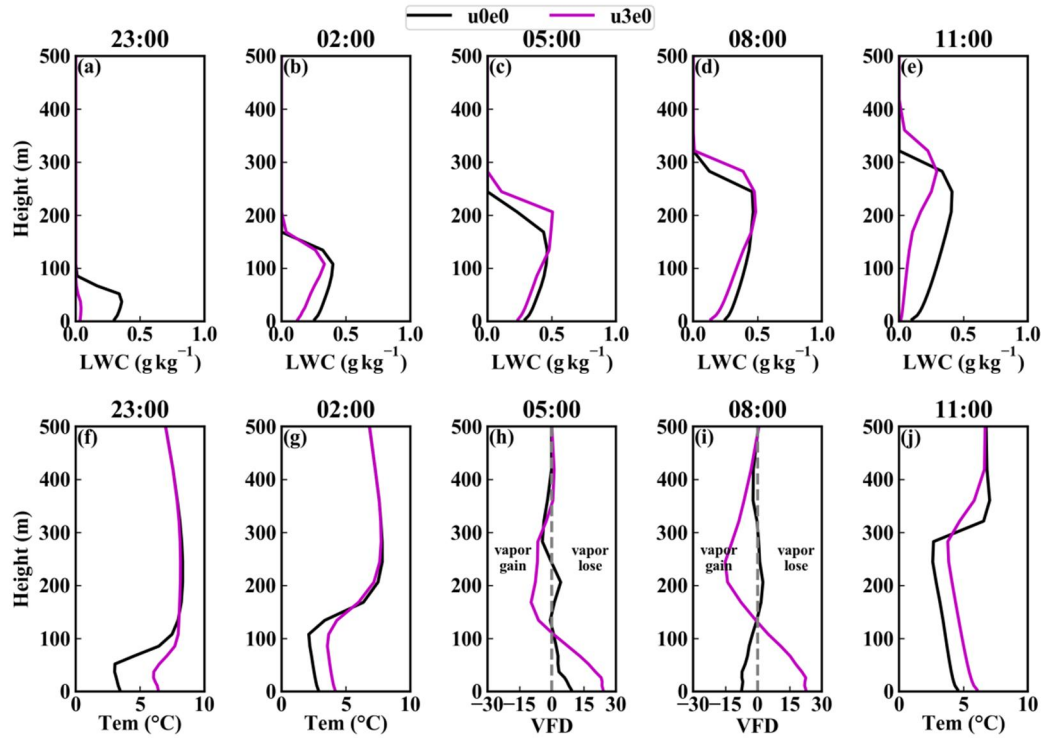
491



493

494 Figure 5. Time-height distribution of the LWC ( $\text{g kg}^{-1}$ ) in (a) u0e0 and (b) u3e0, and (c) is the urbanization effect (u3e0  
 495 minus u0e0) on LWC. The two white curves in (c) are the LWP. The black contour lines in (c) are the difference of  
 496 vertical velocity ( $\text{cm s}^{-1}$ ) (u3e0 minus u0e0). Only the lines after 00:00 are shown for clarity.

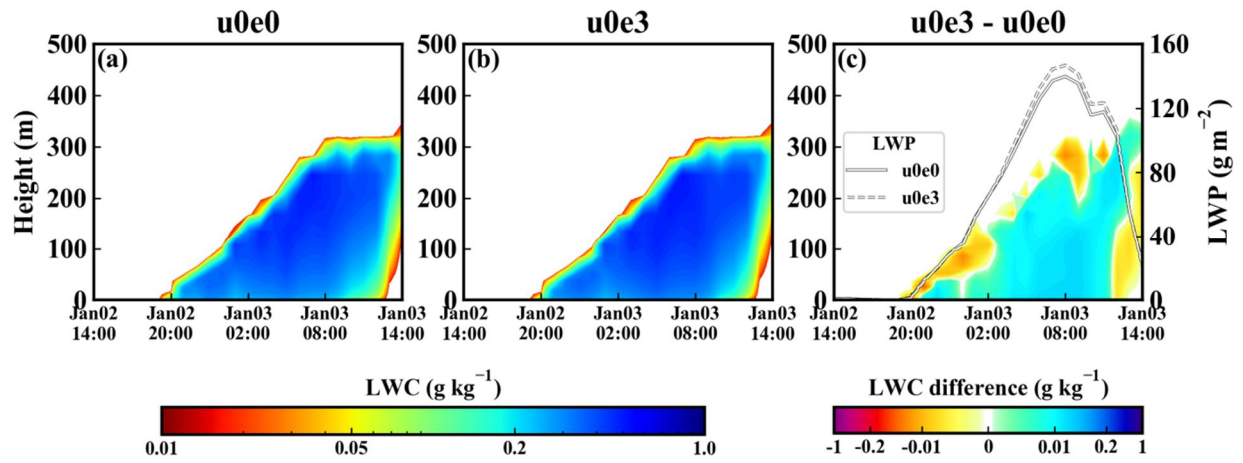
497



499

500 Figure 6. Profiles of the LWC (first row), temperature (Tem) (f, g, j) and vertical vapour flux divergence (VFD) (h, i)  
 501 ( $\text{g h}^{-1} \text{m}^{-2} \cdot \text{hpa}^{-1}$ ) in u0e0 and u3e0 at different times.

502

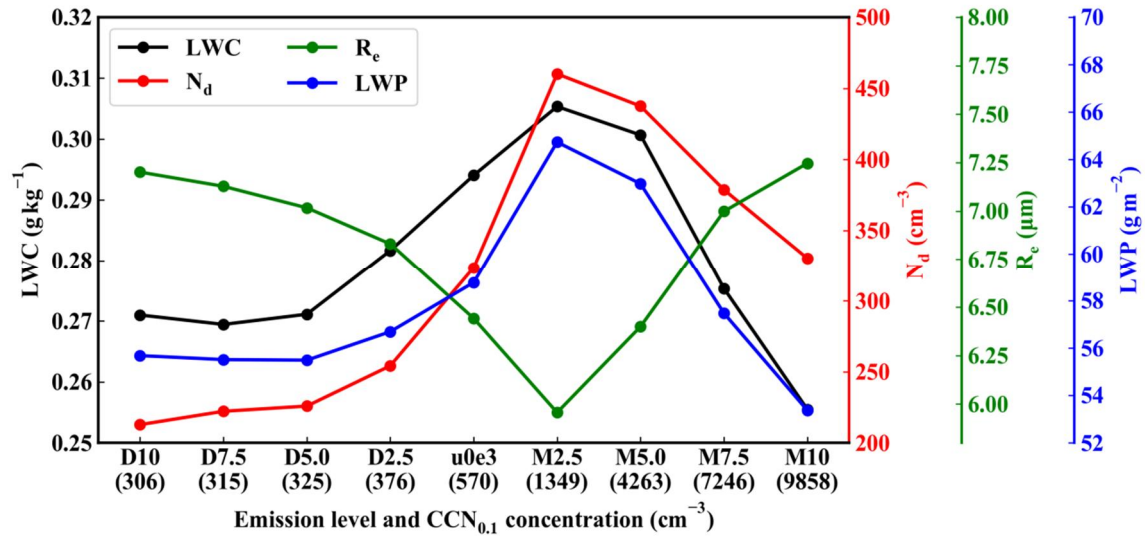


504

505 Figure 7. Similar to Fig. 5, but for the aerosol effect ( $u0e3$  minus  $u0e0$ ).

506

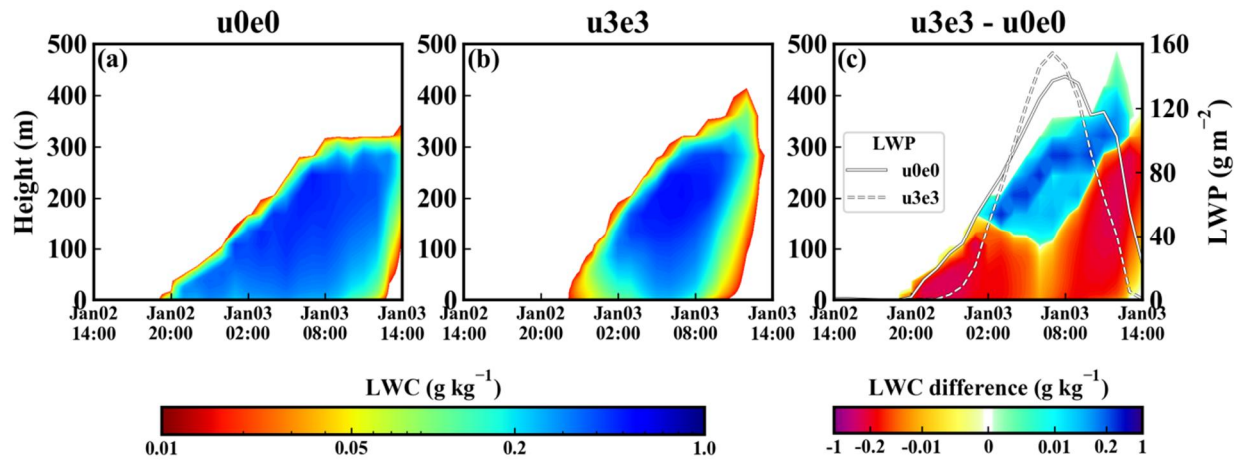




508

509 Figure 8. Relationships of the microphysical parameters (LWC,  $N_d$ ,  $R_e$  and LWP) with emission level and  $CCN_{0.1}$  con-  
 510 centrations. These parameters are the time-height averages (time average for the LWP) in fog.

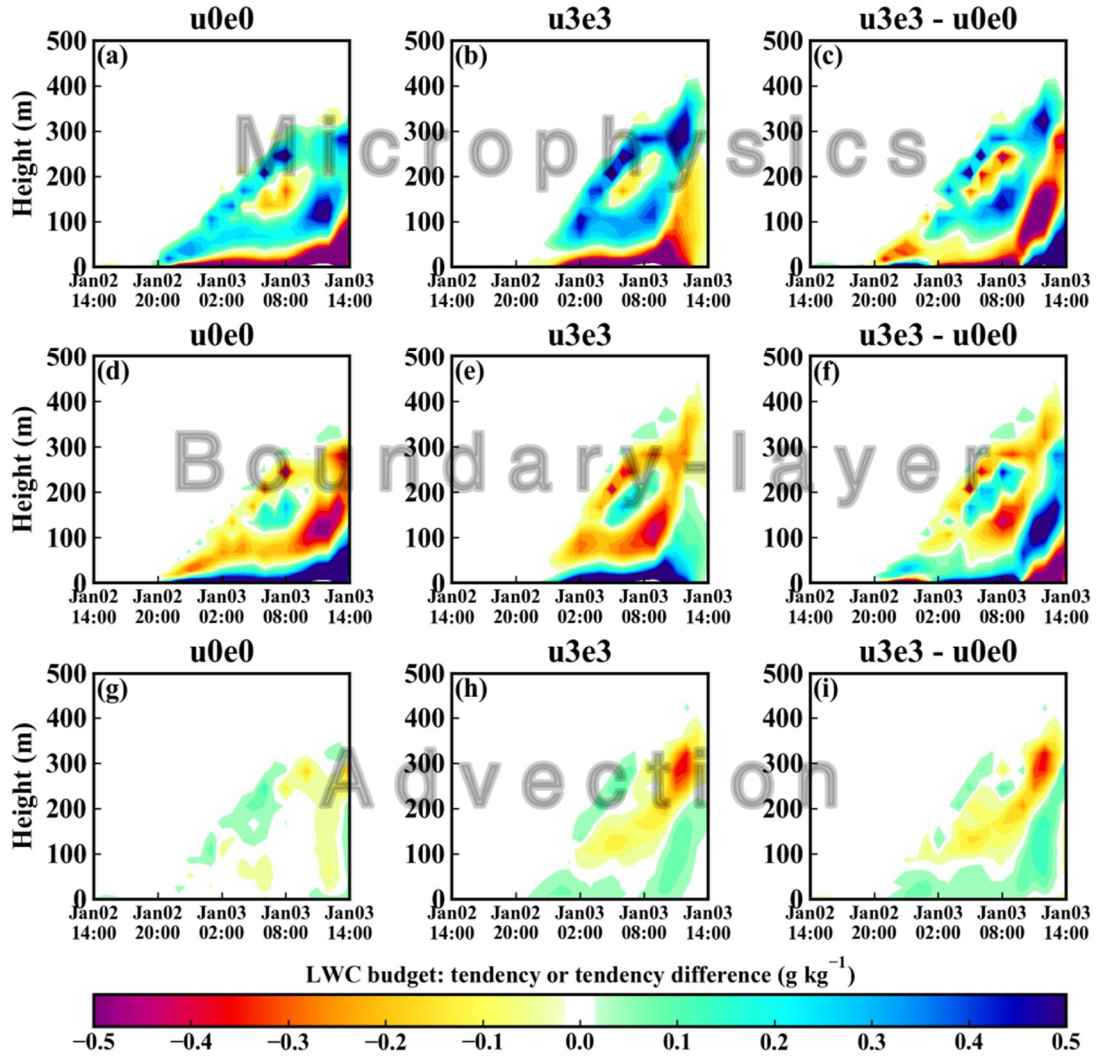
511



513

514 Figure 9. Similar to Fig. 5, but for the combined effect of urbanization and aerosols ( $u3e3$  minus  $u0e0$ ).

515

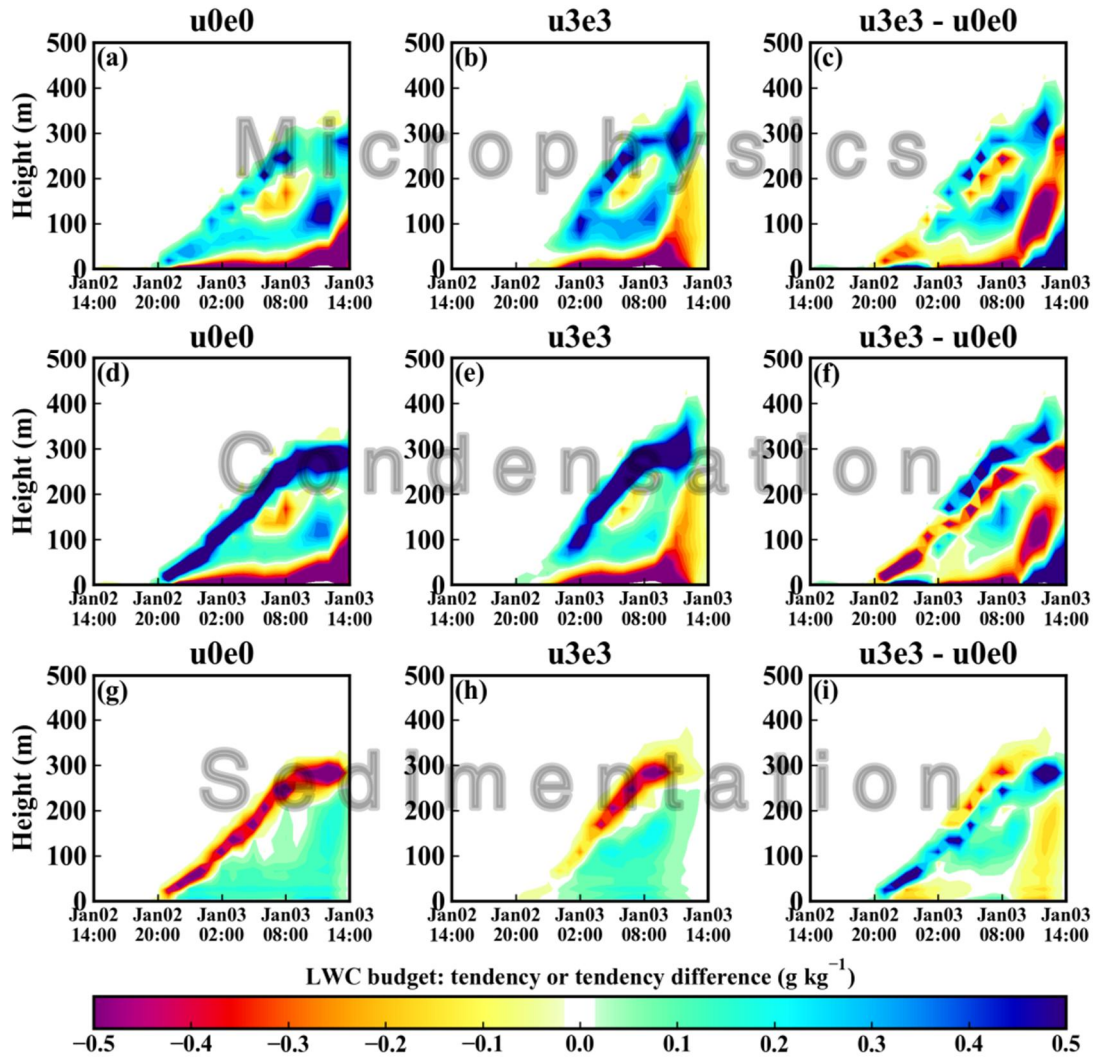


517

518 Figure 10. The combined effect of urbanization and aerosols (u3e3 minus u0e0) on various items of the LWC budget.

519 The three rows are the hourly tendencies (g kg<sup>-1</sup>) of the microphysical, boundary layer, and advection processes.

520



522

523 Figure 11. The combined effect of urbanization and aerosols (u3e3 minus u0e0) on various items of the microphysical  
 524 tendency. The three rows are the hourly tendencies ( $\text{g kg}^{-1}$ ) of the microphysical, condensation/evaporation, and sedi-  
 525 mentation processes.

526